Steel and Composite Structures, *Vol. 28, No. 1 (2018) 39-49*
DOI: https://doi.org/10.12989/scs.2018.28.1.039

Influence of post-pouring joint on long-term performance of steel-concrete composite beam

Dunwen Huang [a], Jun Wei, Xiaochun Liu [*], Shizhuo Zhang and Tao Chen

School of Civil Engineering, Central South University, Changsha, Hunan, 410075, China

(*Received February 12, 2018, Revised April 8, 2018, Accepted April 11, 2018*)

Abstract. The concrete bridge decks are usually precast and in-situ assembled with steel girders with post-pouring joint in the construction practice of super-wide steel-concrete composite beam. But the difference of concrete age between the precast slabs and the post-pouring joint has been not yet considered for the long-term performance analysis of this kind composite beam. A simply supported precast-assembled T-shaped beam was taken as an example to analyze the long-term performance of steel-concrete composite beam with post-pouring joint. Based on the deformation coordination conditions of the old-new concrete deck and steel girder, a theoretical model for the long-term behavior of precast-assembled composite beam is proposed in this paper according to age-adjusted effective modulus method. Then, the feasibility of the proposed model is verified by the available test data from the Gilbert's composite beams. Parametric studies were preformed to evaluate the influences of the cross-sectional area ratio of the post-pouring joint to the whole bridge deck, as well as the difference of concrete age between the precast slabs and the post-pouring joint, on the long-term performance of the composite beam. The results indicate that the traditional method without considering the age difference would seriously underestimate the effect of creep and shrinkage of concrete bridge decks. The concrete age difference between the precast slabs and the post-pouring joint should be demonstrated for the life cycle design and long-term performance analysis of precast-assembled steel-concrete composite beams.

Keywords: composite beam; precast-assembled; post-pouring joint; shrinkage; creep; assembled age

1. Introduction

Due to the advantages of short durance, reduction of construction expense and facility of construction, the precast-assemble construction technology is widely adopted for steel-concrete composite beam project. Most of the concrete bridge decks are usually precast and in-situ assembled with steel girders with post-pouring joint in super-wide steel-concrete composite beam. The precast slabs and the new concrete joint are usually treated to be an integral precast bridge decks for the design and the long-term performance analysis of steel-concrete composite beam in existing studies. The influence of the age difference between the precast concrete slabs and post-pouring joint on the long-term performance of composite beam is ignored in engineering practice.

The long-term performance analysis of steel-concrete composite beam began in the 1980s: Gilbert and Bradford (1989) calculated the creep effect of the composite beam using two approaches: the age-adjusted effective modulus method and Dischinger differential constitutive procedure. And then (1991), they conducted experiments about the long-term performance of composite beam by taking the loads and shear stiffness as variables. Dezi *et al.* (1995, 2006) considered the effect of the pre- stress of the concrete slabs on the shrinkage and creep of composite beam and indicated that the shear lag phenomenon near the pre-stressed anchorage zone is obviously, and the effective width changes by time. Amadio and Fragiacomo (1997) studied deeply the time-dependent behavior of the composite beam of the rigid and flexible shear connector and proposed a simplified calculation method. Giussani and Mola (2010) constructed the long-term deformation calculation model of composite beam considering axial and bending loads based on the previous studies. Gara *et al.* (2010, 2011a, b) introduced the function of the transverse warping displacement considering the shear lag effect into the time-dependent analysis model, and established the cable-stayed bridge model considering the shrinkage and creep effect of composite beam using the finite beam method, and indicated that the effective width of the concrete slab gradually changes by time, and suggested the full width of the concrete slab should be adopted in the analysis of long-term effect. Erkmen and Bradford (2011) proposed a analytical method of curved composite beam with time effect based on the energy variational principle and studied the influence of the curvature, radial and longitudinal shear stiffness on the long-term deformation. Nguyen (Nguyen *et al.* 2010a, b) established the stiffness matrix of the time-dependent analysis of composite beam based on the elastic theory and Kelvin composite viscoelastic creep model and then (Nguyen and Hjiaj 2016) proposed a nonlinear time-dependent analysis method considering the influence of concrete cracking on composite beam based on introducing an elasto-plastic model with

*Corresponding author, Ph.D.,
E-mail: xchliu@csu.edu.cn
[a] Ph.D. Student, E-mail: dunwenhuang@csu.edu.cn

ISSN: 1229-9367 (Print), 1598-6233 (Online)

softening. Wu *et al*. (2015) presented a master-slave constraint method to investigate the time-dependent performance of steel-concrete composite bridges during construction. Deretic-Stojanovic and Kostic (2017) proposed the matrix stiffness method simplified the non-homogeneous integral equations into algebraic equations by introducing the assumption that the unknown deformations change linearly with the concrete creep function. Considering the effects of interface slip, shear-lag and time-dependence, Zhu and Su (2017) presented a novel high-precision solution method based on the closed-form solution of the space domain of the one-dimensional analytical model.

All the above studies have established the model of the time-dependent analysis of the composite beam, but the influence of the age difference between the precast concrete slabs and the post-pouring joint on long-term performance are ignored obviously. However, the width of bridge increases with the needs of urban construction in recent years, and the cross-sectional area ratio of the post-pouring joint to the whole deck of precast-assembled composite beam also increases. Therefore, it is urgent to make clear the effect of post-pouring joint on the long-term performance of composite beam. This paper details the development and application of such a time-dependent model with considering the age difference effect of post-pouring joint.

2. Instantaneous model of steel-concrete composite beam

2.1 Principle assumptions

A large number of experiments research (Xue *et al*. 2008, 2013, Fan *et al*. 2010a, b, Al-Deen *et al*. 2011a, b, 2015) have confirmed that the steel girder, concrete slabs and steel-concrete interface are basically in the elastic working stage under action of the service load. To simplify the analysis and the calculation process, the following assumptions are proposed:

(1) The deformation of the concrete slab and steel girder of composite beam conform to the plane cross-section assumption;

(2) The shear stress of steel-concrete interface τ is directly proportional to the relative slip S between these two layers, namely

$$\tau = kS$$

where k refers to the average shear stiffness of the composite beam.

(3) The vertical uplift effect of the composite beam is neglected, and the curvature of the steel girder is considered to be the same with that of the concrete slabs.

2.2 Mechanical model

For typical steel-concrete composite beam, the equilibrium of forces in an infinitesimal beam adopting the free-body method is given in Fig. 1.

In Fig. 1, according to the equilibrium condition of forces in the free body of the whole concrete slab and steel girder, one obtained

$$\begin{cases} \dfrac{dN_c}{dx} = -\tau \\ \dfrac{dN_s}{dx} = \tau \end{cases} \tag{1}$$

$$\frac{dM_c}{dx} + \frac{dM_s}{dx} = V_c + V_s - \frac{h}{2}\tau \tag{2}$$

$$\frac{dV_c}{dx} + \frac{dV_s}{dx} = -q \tag{3}$$

where N, M, V and q refers to the axial force, bending moment, shear force and uniform distribution load, respectively. The subscript c, s and P in Eqs. (1)-(3) denotes concrete slab, steel girder and prestressing tendon, respectively. In addition, h is the depth of the composite beam, $h = h_c + h_s$, where h_c and h_s is the depth of the concrete slab and that of steel girder, respectively.

Based on the previously mentioned assumptions, the curvature of the steel girder and concrete slab can be expressed as

$$w'' = \frac{M_c}{E_c I_c} = \frac{M_s}{E_s I_s} \tag{4}$$

where $I_0 = I_c / n + I_s$, $n = E_s / E_c$ and w, E, I are the deflection of composite beam, elastic modulus and moment of inertia, respectively.

Making use of Eqs. (2) and (4), the governing differential equation for the deformation of composite beam can be obtained

$$E_s I_0 w^{(4)} = -q - \frac{kh}{2} S' \tag{5}$$

The relative slip of steel-concrete interface can be deduced from the deformation coordination

$$S' = \frac{N_s}{E_s A_s} - \frac{N_c}{E_c A_c} - \frac{h}{2} w'' \tag{6}$$

Submit Eq. (1) into the equation obtained after the derivation of Eq. (6), and then we have

$$S'' = mS - \frac{h}{2} w''' \tag{7}$$

where

$$m = k(1/E_s A_s + 1/E_c A_c)$$

According to Eqs. (5) and (7), the interfacial slip of steel-concrete and the instantaneously deflection of the composite beam subject to uniformly distributed load are as follows

$$S_0 = \frac{C_1 e^{\gamma_0 x} - C_2 e^{-\gamma_0 x}}{r_0} - B_2 x + C_3 \tag{8}$$

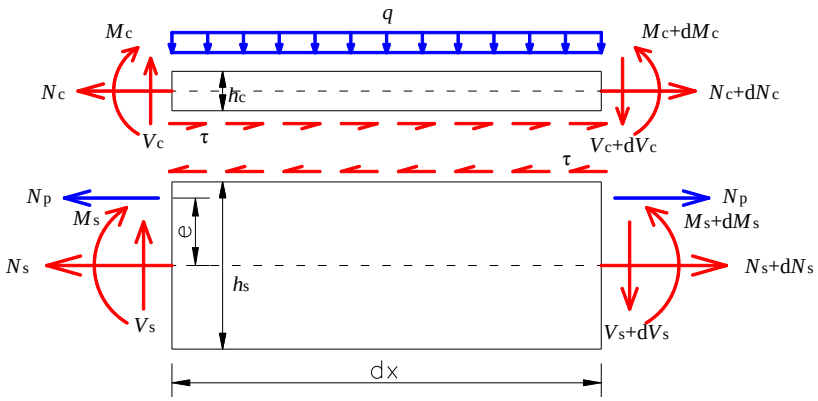

Fig. 1 The equilibrium of forces of infinitesimal beam

$$w_0 = -\frac{kh}{2E_sI_0r_0^4}(C_1e^{\gamma_0 x} + C_2e^{-\gamma_0 x}) - \frac{1}{24E_sI_0}(q - \frac{kh}{2}B_2)x^4 + \frac{1}{6}C_4x^3 + \frac{1}{2}C_5x^2 + C_6x + C_7 \quad (9)$$

where

$$\gamma_0 = \sqrt{m + kh^2 / 4E_sI_0}$$

$$B_1 = -N_p(\frac{1}{E_sA_s} + \frac{h}{2}\frac{e_p}{E_sI_0})$$

$$B_2 = \frac{q}{kh/2 + 2mE_sI_0/h}$$

According to the boundary conditions of simply supported composite beam, it can be obtained that

$$\begin{cases} w(0) = w(L) = 0 \\ S(L/2) = 0 \end{cases}$$

In addition, the expression of total bending moment of steel-concrete composite beams is

$$M(x) = M_c + M_s - N_ch/2 - N_pe_p$$

And combine Eq. (4), it can be deduced that

$$w''(0) = w''(L) = \frac{N_pe_p}{E_sI_0}$$

According to Eq. (6), one obtain

$$S'(0) = S'(L) = B_1$$

Combine the above mentioned general solution of differential equations and the corresponding boundary conditions, we have the expressions for C_1-C_7 as

$$C_1 = \frac{1 - e^{-\gamma_0 L}}{e^{\gamma_0 L} - e^{-\gamma_0 L}}(B_1 + B_2)$$

$$C_2 = \frac{e^{\gamma_0 L} - 1}{e^{\gamma_0 L} - e^{-\gamma_0 L}}(B_1 + B_2)$$

$$C_3 = \frac{L}{2}B_2 - \frac{C_1e^{\gamma_0 L/2} - C_2e^{-\gamma_0 L/2}}{\gamma_0}$$

$$C_4 = \frac{L}{2E_sI_0}\left(q - \frac{kh}{2}B_2\right)$$

$$C_5 = \frac{N_pe_p}{E_sI_0} + \frac{kh}{2E_sI_0\gamma_0^2}(B_1 + B_2),$$

$$C_6 = \frac{-N_pe_pL}{2E_sI_0} - \frac{L^3}{24E_sI_0}\left(q - \frac{kh}{2}B_2\right) - \frac{khL}{4E_sI_0\gamma_0^2}(B_1 + B_2),$$

$$C_7 = \frac{kh}{2E_sI_0\gamma_0^4}(B_1 + B_2)$$

Based on the expression of the axial force, which deduced by integrating the equation acquired by substituting Eq. (8) into Eq. (1), and the boundary condition of $N_c(0) = 0$, one can obtain

$$N_{c0} = -\frac{k}{\gamma_0^2}\left(C_1e^{\gamma_0 x} + C_2e^{-\gamma_0 x}\right) + \frac{k}{2}B_2x^2 - kC_3x + \frac{k}{\gamma_0^2}(C_1 + C_2) \quad (10)$$

$$N_{s0} = -N_{c0} - N_p \quad (11)$$

Eqs. (9)-(11) are submitted into strain expressions in Eqs. (12)-(13), the longitudinal strain in any position of the composite beam can be obtained as

$$\varepsilon_{c0} = \frac{N_{c0}}{E_cA_c} - Z_cw_0'' \quad (12)$$

$$\varepsilon_{s0} = \frac{N_{s0}}{E_sA_s} - Z_sw_0'' \quad (13)$$

where Z_c and Z_s is vertical coordinates of the local coordinate system, and the origin of which are on the neutral axis of the concrete slabs and the steel girder, respectively.

3. Time-dependent mechanical model of precast-assembled composite beam

3.1 Time-dependent model

The principle assumptions of elastic model for steel-concrete composite beam are also suit for the time-dependent model. And it is assumed that the connections between the precast slabs and the post-pouring joint are rigid and none relative slip happens on their interface. The typical schematic of precast-assembled steel-concrete composite beam is given in Fig. 2.

From Fig. 2, it can be seen that the internal force of the concrete slabs is divided into two parts: the precast concrete slabs and longitudinal post-pouring joint. Considering the age effect of concrete and making using of the equation in incremental form proposed by Trost – Bazant (1972), Eqs. (1)-(4) can be rewritten as

$$\begin{cases} \dfrac{2d\Delta N_{ct1}+d\Delta N_{ct2}}{dx}=-\Delta\tau_t \\ \dfrac{d\Delta N_{st}}{dx}=\Delta\tau_t \end{cases} \tag{14}$$

$$\frac{2d\Delta M_{ct1}+d\Delta M_{ct2}}{dx}+\frac{d\Delta M_{st}}{dx}=2\Delta V_{ct1}+\Delta V_{ct2}+\Delta V_{st}-\frac{h}{2}\Delta\tau_t \tag{15}$$

$$\frac{2d\Delta V_{ct1}+d\Delta V_{ct2}}{dx}+\frac{d\Delta V_{st}}{dx}=0 \tag{16}$$

$$\begin{cases} \Delta w_t''=\dfrac{\Delta M_{ct1}}{E_{ct1}(t)I_{c1}}+\dfrac{M_{c1}}{E_cI_{c1}}\phi_1(t,t_1) \\ \quad=\dfrac{\Delta M_{ct2}}{E_{ct2}(t)I_{c2}}+\dfrac{M_{c2}}{E_cI_{c2}}\phi_2(t,t_2) \\ \Delta w_t''=\dfrac{\Delta M_{st}}{E_sI_s} \end{cases} \tag{17}$$

where the subscripts ct1, ct2 denotes the precast concrete slabs and the post-pouring joint, respectively. $\chi_1(t)$, $\chi_2(t)$ and $\phi(t, t_1)$, $\phi_2(t, t_2)$ is aging coefficient and creep coefficient of the precast slabs and the post-pouring joint, respectively. The elastic modulus of the precast slabs and the post-pouring joint is adjusted considering the age effect, and the uniform expression is

$$E_{ct}=E_c/\left[1+\chi(t)\phi(t,t_0)\right]$$

Based on Eqs. (14)-(17), the following simplified equation is obtained

$$\alpha_t\Delta w_t^{(4)}+\frac{kh}{2}\Delta S_t'=\beta_t w_0^{(4)} \tag{18}$$

where

$$\alpha_t=2E_{ct1}(t)I_{c1}+E_{ct2}(t)I_{c2}+E_sI_s$$

$$\beta_t=2E_{ct1}(t)I_{c1}\phi_1(t,t_1)+E_{ct2}(t)I_{c2}\phi_2(t,t_2)$$

On the other hand, based on Eq. (6), the following equation is obtained considering the age effect of concrete

$$\Delta S_t'=\frac{\Delta N_{st}}{E_sA_s}-\frac{\Delta N_{ct2}}{E_{ct2}(t)A_{c2}}-\frac{N_{c2}}{E_cA_{c2}}\phi_2(t,t_2)-\frac{h}{2}\Delta w_t''-\varepsilon_{sh2}(t) \tag{19}$$

According to the deformation coordination condition of the precast concrete slabs and longitudinal post-pouring joint, the following equations are given

$$\frac{N_{c1}}{E_cA_{c1}}=\frac{N_{c2}}{E_cA_{c2}} \tag{20}$$

$$\begin{aligned} &\frac{\Delta N_{ct1}}{E_{ct1}(t)A_{c1}}+\frac{N_{c1}}{E_cA_{c1}}\phi_1(t,t_1)+\Delta\varepsilon_{sh1}(t) \\ &=\frac{\Delta N_{ct2}}{E_{ct2}(t)A_{c2}}+\frac{N_{c2}}{E_cA_{c2}}\phi_2(t,t_2)+\varepsilon_{sh2}(t) \end{aligned} \tag{21}$$

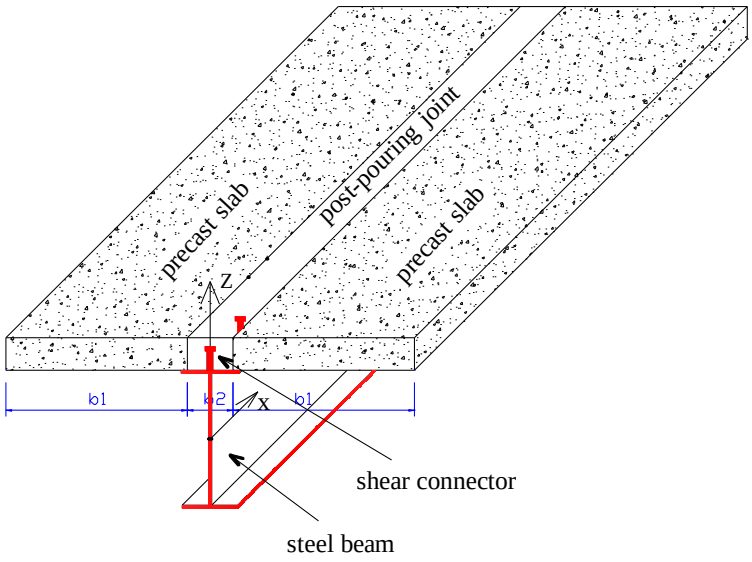

Fig. 2 Schematic of precast-assembled steel-concrete composite beam

According to Eqs. (20), (21), (14) and (1), the following equation is obtained

$$\frac{d\Delta N_{ct2}}{dx}=\frac{2\dfrac{E_{ct1}(t)A_{c1}}{E_cA_c}\left[\phi_2-\phi_1\right]kS_0-k\Delta S_t}{2\dfrac{E_{ct1}(t)A_{c1}}{E_{ct2}(t)A_{c2}}+1} \tag{22}$$

Eq. (22) is submitted into the equation obtained after the derivation of Eq. (6), and then

$$\Delta S_t^{''}-m_t\Delta S_t+\frac{h}{2}\Delta w_t^{'''}=\eta kS_0 \tag{23}$$

where

$$m_t=\frac{k}{E_sA_s}+\frac{k}{2E_{ct1}(t)A_{c1}+E_{ct2}(t)A_{c2}}$$

$$\eta_t=\frac{1}{E_cA_c}\left\{\phi_2-\frac{2E_{ct1}(t)A_{ct1}\left[\phi_2-\phi_1\right]}{2E_{ct1}(t)A_{c1}+E_{ct2}(t)A_{c2}}\right\}$$

Based on Eqs. (18) and (23), and the boundary conditions of simply supported composite beam

$$\begin{cases}\Delta w(0,t)=\Delta w(L,t)=0\\ \Delta S(L/2,t)=0\\ \Delta w''(0,t)=\Delta w''(L,t)=\dfrac{\Delta N_pe_p+N_pe_p\beta_t/E_sI_0}{\alpha_t}\\ \Delta S'(0,t)=\Delta S'(L,t)=\dfrac{2(\varepsilon_{sh2}-\Delta\varepsilon_{sh1})E_{ct1}A_{c1}}{2E_{ct1}A_{c1}+E_{ct2}A_{c2}}-\varepsilon_{sh2}-\dfrac{\Delta N_p}{E_sA_s}-\dfrac{\Delta N_pe_ph+\beta_tN_pe_ph/E_sI_0}{2\alpha_t}\end{cases}$$

one obtained

$$\begin{aligned}\Delta S_t=&\frac{1}{\lambda_t}\left(C_8e^{\lambda_tx}-C_9e^{-\lambda_tx}\right)\\&+\frac{1}{\gamma_0}\left(a_1e^{\gamma_0x}-a_2e^{-\gamma_0x}\right)+a_3x+C_{10}\end{aligned} \tag{24}$$

$$\begin{aligned}\Delta w_t=&\frac{B_5}{\gamma_0^4}(C_1e^{\gamma_0x}+C_2e^{-\gamma_0x})+\frac{B_6}{\lambda_t^4}(C_8e^{\lambda_tx}+C_9e^{-\lambda_tx})\\&+\frac{1}{12h}(m_ta_3-\eta_tkB_2)x^4+\frac{1}{6}C_{11}x^3+\frac{1}{2}C_{12}x^2+C_{13}x+C_{14}\end{aligned} \tag{25}$$

where

$$\lambda_t=\sqrt{m_t+kh^2/4\alpha_t}$$

$$a_1=\frac{-2C_1h}{4\alpha_t(m_t-\gamma_0^2)+kh^2}B_3$$

$$a_2=\frac{-2C_2h}{4\alpha_t(m_t-\gamma_0^2)+kh^2}B_3$$

$$a_3=\frac{2h(B_2B_3-q\beta_t/E_sI_0)}{4\alpha_tm_t+kh^2}$$

$$B_3=\frac{2\alpha_t\eta_tk}{h}+\frac{kh\beta_t}{2E_sI_0}$$

$$B_4=\frac{2(\varepsilon_{sh2}-\Delta\varepsilon_{sh1})E_{ct1}A_{c1}}{2E_{ct1}A_{c1}+E_{ct2}A_{c2}}-\varepsilon_{sh2}-\frac{\Delta N_p}{E_sA_s}-\frac{\Delta N_pe_ph+\beta_tN_pe_ph/E_sI_0}{2\alpha_t}$$

$$B_5=\frac{2\eta_tk}{h}-\frac{4\left(m_t-\gamma_0^2\right)}{4\alpha_t(m_t-\gamma_0^2)+kh^2}B_3$$

$$B_6=\frac{2}{h}\left(m_t-\lambda_t^2\right)$$

$$C_8=\frac{1-e^{-\lambda_tL}}{e^{\lambda_tL}-e^{-\lambda_tL}}\left(B_4-a_3\right)+\frac{e^{-\lambda_tL}-e^{\gamma_0L}}{e^{\lambda_tL}-e^{-\lambda_tL}}a_1+\frac{e^{-\lambda_tL}-e^{-\gamma_0L}}{e^{\lambda_tL}-e^{-\lambda_tL}}a_2$$

$$C_9=\frac{e^{\lambda_tL}-1}{e^{\lambda_tL}-e^{-\lambda_tL}}\left(B_4-a_3\right)-\frac{e^{\lambda_tL}-e^{\gamma_0L}}{e^{\lambda_tL}-e^{-\lambda_tL}}a_1-\frac{e^{\lambda_tL}-e^{-\gamma_0L}}{e^{\lambda_tL}-e^{-\lambda_tL}}a_2$$

$$C_{10}=-\frac{1}{\lambda_t}\left(C_8e^{\lambda_tL/2}-C_9e^{-\lambda_tL/2}\right)-\frac{1}{\gamma_0}\left(a_1e^{\gamma_0L/2}-a_2e^{-\gamma_0L/2}\right)-\frac{L}{2}a_3$$

$$C_{11}=-\frac{B_6}{\lambda_t^2L}\left[a_1\left(1-e^{\gamma_0L}\right)+a_2\left(1-e^{-\gamma_0L}\right)\right]-\frac{L}{h}\left(m_ta_3-\eta_tkB_2\right)$$

$$C_{12}=\frac{\Delta N_pe_p+N_pe_p\beta_t/E_sI_0}{\alpha_t}-\frac{B_5}{\gamma_0^2}\left(B_1+B_2\right)-\frac{B_6}{\lambda_t^2}\left(B_4-a_1-a_2-a_3\right)$$

$$C_{13}=\frac{\lambda_t^2L^2-6}{6\lambda_t^4L}\left[a_1\left(1-e^{\gamma_0L}\right)+a_2\left(1-e^{-\gamma_0L}\right)\right]B_6+\frac{L^3}{12h}\left(m_ta_3-\eta_tkB_2\right)-\frac{L}{2}C_{12}$$

$$C_{14}=-\frac{B_5}{\gamma_0^4}\left(B_1+B_2\right)-\frac{B_6}{\lambda_t^4}\left(B_4-a_1-a_2-a_3\right)$$

Eqs. (8) and (24) are submitted into Eq. (22).And then, combined Eq. (21) with the following boundary condition

$$\Delta N_{ct}(0)=2\Delta N_{ct1}(0)+\Delta N_{ct2}(0)=0$$

The increment of axial force ΔN_{ct2} and ΔN_{st} can be written as

$$\begin{aligned}\Delta N_{ct2}=&-\frac{2\dfrac{E_{ct1}A_{c1}}{E_cA_c}(\phi_2-\phi_1)}{2\dfrac{E_{ct1}A_{c1}}{E_{ct2}A_{c2}}+1}N_{c0}-\frac{k}{2\dfrac{E_{ct1}A_{c1}}{E_{ct2}A_{c2}}+1}\cdot\\&\left(\begin{array}{l}\dfrac{C_8e^{\lambda_tx}+C_9e^{-\lambda_tx}}{\lambda_t^2}+\dfrac{a_1e^{\gamma_0x}+a_2e^{-\gamma_0x}}{\gamma_0^2}+\dfrac{a_3}{2}B_2x^2+\\ C_{10}x+\dfrac{2E_{ct1}A_{c1}}{k}(\varepsilon_{sh2}-\Delta\varepsilon_{sh1})-\dfrac{C_8+C_9}{\lambda_t^2}-\dfrac{a_1+a_2}{\gamma_0^2}\end{array}\right)\end{aligned} \tag{26}$$

$$\Delta N_{st}=-\left(2\Delta N_{ct1}+\Delta N_{ct2}\right)-\Delta N_p \tag{27}$$

where ΔN_{ct1} can be obtained by Eq. (26) and (21). Likewise, the increment of longitudinal strain at any position of the composite beam can be obtained by

$$\Delta\varepsilon_{ct}=\frac{\Delta N_{ct2}}{E_{ct2}A_{c2}}+\frac{N_{c0}}{E_cA_c}\phi_2+\varepsilon_{sh2}-Z_c\Delta w_t'' \tag{28}$$

$$\Delta\varepsilon_{st}=\frac{\Delta N_{st}}{E_sA_s}-Z_s\Delta w_t'' \tag{29}$$

According to Trost-Bazant's (Bazant 1972) creep stress-strain equation in algebraic form, the longitudinal stress of concrete at any position of the composite beam can be obtained

$$\sigma_{ct} = \varepsilon_{c0}\left[E_c - E_{ct}\phi(t,t_0)\right] + E_{ct}\left[\Delta\varepsilon_{ct} - \varepsilon_{sh}\right] \tag{30}$$

3.2 Calculation process

Based on the elastic model and the time-dependent model of the precast-assembled steel-concrete composite beam, the long-term performance of the composite beam can be predicted following the flow chart as given in Fig. 3. A calculation program for the long-term performance of the composite beam is compiled in MAPLE. In addition, the structural behavior of the precast-assembled steel-concrete composite beam at any time can be predicted by the program.

3.3 Verification

To verify the feasibility of the incremental differential method in the creep and shrinkage deformation analysis of the precast-assembled steel-concrete composite beam, we related the test results of precast-assembled composite beam. Since none of related test result is available currently, reliable test results of the composite beam with integral concreting were adopted. The composite beam with integral concreting is particular case on the boundary of the proposed model, where the age and creep coefficient and shrinkage strain of the precast slabs and the post-pouring joint are identical among Eqs. (25), (28) and (29).

Gilbert and Bradford's test (1991) is usually adopted to evaluate the model for steel-concrete composite beam. Comparison analysis was conducted between the calculated results of the proposed method in this paper and test data from Gilbert and Bradford's (1991) steel-concrete composite beam. The dimensions of the typical composite beam are shown in Fig. 4. The width and length of the test beam B1 to B4 are 1 m and 5.9 m, respectively. And after 10 days' curing of concrete, the test beam B1 and B3 were loaded with a sustained uniformly distributed load of 7.52 kN/m, while the other beams B2 and B4 were subjected to self-weight only. Furthermore, the pairs of shear connectors were welded at 200 mm intervals in beams B1, B2, and at 600 mm intervals in beams B3, B4. The stiffness of a shear stud deduced by the authors from the push-out resulting curves was 84 kN/mm. The composite beams are assumed to be elastic, with elastic modulus of the concrete and steel girder was 25.1 GPa (t = 10d) and 200 GPa, respectively. The creep and shrinkage functions of concrete for the proposed model were taken as CEB-FIP MC90, the relative humidity RH is 50%, and the compressive strength of concrete f_{ck} is 31.1 MPa.

The comparison results between the measured deflection and strain of the test beam and the calculated results of the proposed method are shown in Figs. 5-6. It can be seen that the deflection and longitudinal strain calculated by the proposed method agree well with Gilbert and Bradford's test results. The calculated response of the composite beams under only gravity from the proposed model slightly differs from the experimental results. Similar phenomenon has been described by Jurkiewiez *et al*. (2005), which can be

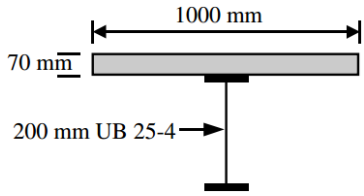

Fig. 4 Tested beams by Gilbert and Bradford (1991)

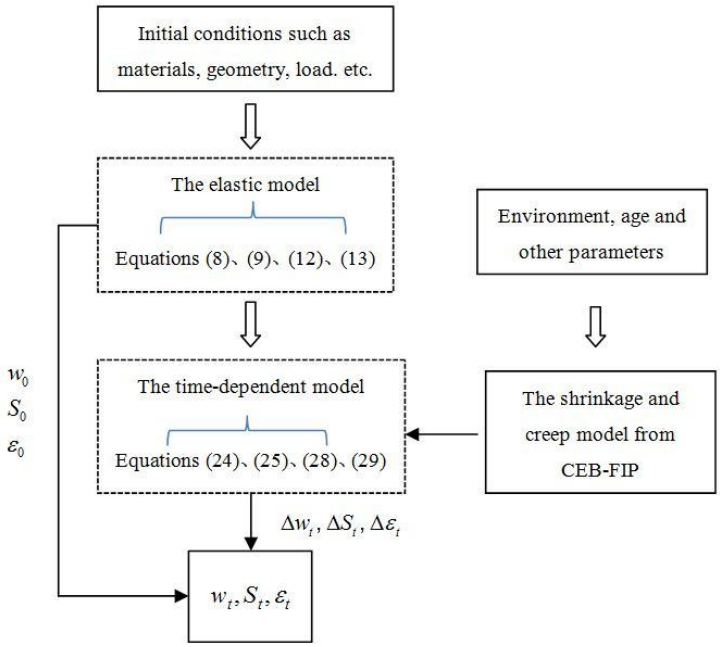

Fig. 3 The calculation flow chart

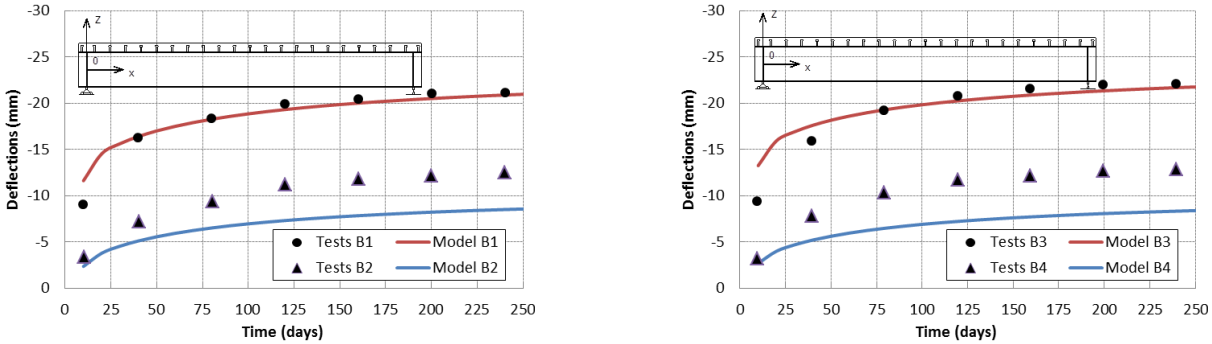

Fig. 5 Comparison of the calculated mid-span deflections with test results

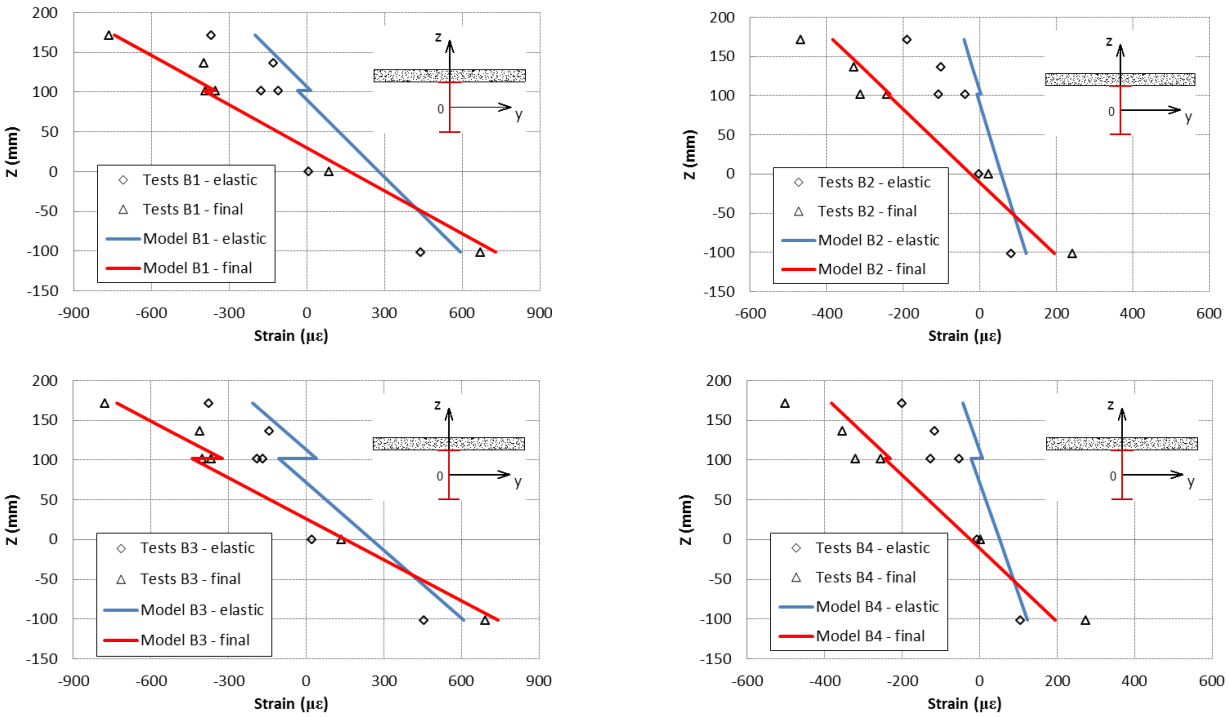

Fig. 6 Comparison of the calculated cross-sectional strain with test results

explained as the long-term behavior in their study were mainly influenced by shrinkage, and the parameters of the shrinkage function were unknown. Therefore, the proposed model in this paper is feasible for the long-term performance prediction of precast-assembled steel-concrete composite beam.

4. Case analysis

Qingshan bridge is a precast-assembled steel-concrete composite beams across Yongjiang River in Nanning city, China. To evaluate the influence of longitudinal post-pouring joint on long-term performance of composite beam, a series of precast-assembled composite beam specimens with the same parameters, such as the ratio of bending and compression stiffness of steel to concrete, the shear surface ratio of shear studs to composite beam and the cross-sectional area ratio of the longitudinal post-pouring joint to the whole concrete slab, with Qingshan bridge were designed as shown in Fig. 7. Herein, the theoretical analysis for precast-assembled steel-concrete composite beams is carried out and the relevant experimental results would be reported later after finished the test. To make a comparative analysis, the shrinkage of concrete before assembly is deducted for the proposed model and the traditional analysis without considering the age difference between the precast slabs and the post-pouring joint.

All the precast concrete slabs were assembled into the whole bridge deck with post-pouring joint at the age of 180 days, and 10 days of natural curing of concrete was conducted after the placement of joint. Two different kinds of load mode are applied in this study: case 1 is under a sustained uniformly distributed load of 5 kN/m; case 2 is under a concentrated axial force of 90 kN which is applied on the position of 225 mm under the top of the steel girder. The strength grade of concrete is C50 for both the precast concrete slabs and the post-pouring joint, and the corresponding elastic modulus of the concrete is 34.5 GPa. The elastic modulus of the steel girder is 210 GPa, and the

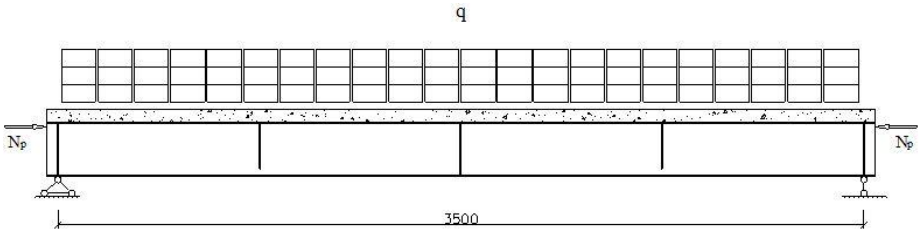

(a) Elevation view

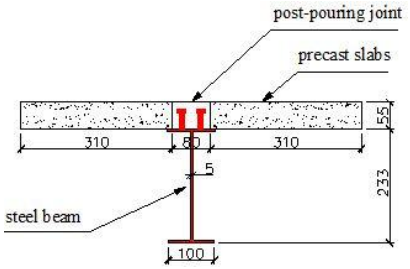

(b) Cross-sectional view

Fig. 7 Diagram of example beam

average shear stiffness of the composite beam is 3623.5 N/mm$^{2.}$ Annual average relative humidity of the environment is taken as 70% according to meteorological record of Nanning, and the creep coefficient and the model of shrinkage deformation are obtained according to CEB-FIP MC90. The mid-span deflection, the strain of concrete and steel, and the slip at end of composite beam calculated by proposed this model and traditional analysis are

Table 1 Comparison of key data under uniform load

Items		Elasticity	360 days			3600 days		
			Traditional method ①	Proposed method ②	$\frac{②-①}{①}$	Traditional method ①	Proposed method ②	$\frac{②-①}{①}$
concrete strain ($\mu\varepsilon$)	Top	-45	-103	-129	24.3%	-150	-176	17.3%
	Bottom	-5	-49	-68	39.0%	-84	-104	23.5%
Steel strain ($\mu\varepsilon$)	Top	-11	-55	-74	35.0%	-90	-110	22.0%
	Bottom	159	176	182	3.5%	187	194	3.4%
Maximum slip (mm)		0.009	0.003	-0.001	-141.2%	-0.004	-0.009	108.5%
Deflection (mm)		-0.933	-1.297	-1.458	12.4%	-1.590	-1.757	10.5%

*Note: The strain and deflection are corresponding to the mid-span of beam

Table 2 Comparison of key data under axial load

Items		Elasticity	360 days			3600 days		
			Traditional method ①	Proposed method ②	$\frac{②-①}{①}$	Traditional method ①	Proposed method ②	$\frac{②-①}{①}$
concrete strain ($\mu\varepsilon$)	Top	-43	-124	-150	21.5%	-177	-204	15.6%
	Bottom	-50	-111	-131	18.2%	-152	-173	13.9%
Steel strain ($\mu\varepsilon$)	Top	-50	-111	-131	18.2%	-152	-173	13.9%
	Bottom	-76	-58	-52	-11.0%	-45	-38	-15.0%
Maximum slip (mm)		0.093	0.084	0.080	-5.3%	0.076	0.071	-6.2%
Deflection (mm)		0.100	-0.408	-0.579	41.9%	-0.751	-0.929	23.8%

*Note: The strain and deflection are corresponding to the mid-span of beam

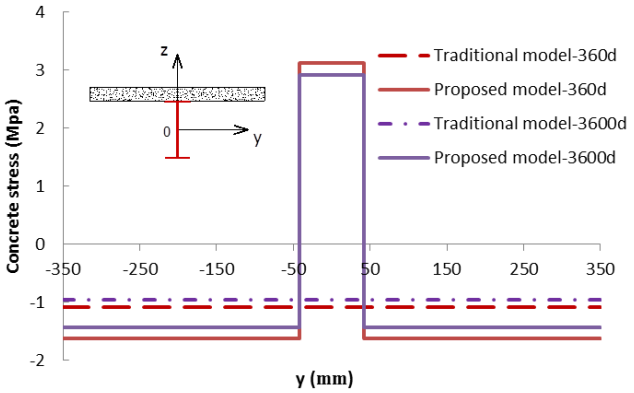

Fig. 8 Cross-section distribution of longitudinal stress under uniform vertical load

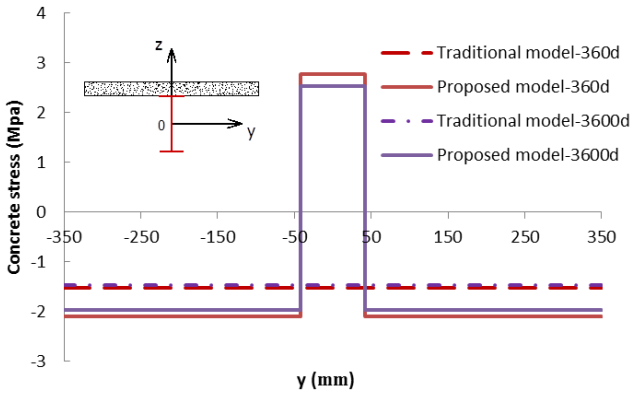

Fig. 9 Cross-section distribution of longitudinal stress under axial load

presented in Tables 1-2. The distribution of longitudinal stress on the top surface along the width of concrete slab predict by the proposed model is shown in Figs. 8-9.

It can be seen from Table 1 that the concrete strains and mid-span deflection of the composite beam that subjected to vertical uniformly distributed load gradually increase, while the maximum interface slip decrease with time according to the two models. The values of concrete strains and mid-span deflection calculated by the proposed model are much larger than that of traditional model, and the difference of values calculated by the two models gradually decrease with time. For the case study, the difference of calculated value for maximum longitudinal concrete strain is 24.3% and 17.3% at the age of one year and ten years, respectively. And the corresponding difference of calculated value for mid-span deflection is 12.4% and 10.5% at the age of one year and ten years, respectively. It should be noted that the difference of the maximum tensile strain at the bottom of steel girder calculated by the two models is very small, which indicates that the effect of age difference on steel girder can be ignored. Although the difference of the maximum slip calculated by the two models is large, too small interface slip has no practical significance.

The calculated values given in Table 2 demonstrated the variations of concrete strains and mid-span deflection and the maximum slip of the composite beam under axial load with time are similar to the case of uniformly distributed vertical load. However, the calculated values for concrete and steel strain on steel-concrete interface and the maximum slip given in Table 2 are much higher than that in Table 1. The difference of the two models is reduced to less than 18% and 6% for interfacial concrete strain and the maximum slip, respectively. Unlike the case under the action of the uniform vertical load, the difference of the mid-span deflection calculated by the proposed model and traditional model at the age of 10 years is still 23.8%, but the value of deflection is small.

Figs. 8-9 show that the concrete stress of the top deck calculated by the two models decreases with time, and the value calculated by the proposed model is much greater than the traditional model. For the cases under the action of uniform vertical load and the axial load, the concrete stress calculated by the proposed model are 49% and 36% larger than those of the traditional model, respectively, which indicates that the effect of post-pouring joint delays the transformation of the stress from the concrete slabs to the steel girder. It should be noted that the tensile stress can be formed in the post-pouring joint according the proposed model that consider the age different, which is much different with the case of traditional model. Based on Eq. (30), it can be found the reason that the shrinkage strain ε_{sh} of the post-pouring joint is larger than the total strain $\varepsilon_{c0} + \Delta\varepsilon_{ct}$ of the concrete slabs. In addition, the value of the tensile stress decreases slightly with time.

5. Influence of post-pouring joint

According to the time-related parameters α_t, β_t, m_t, η_t and ε_{sh} in Section 3.1, the parameter of the assembled age (t_a) and the cross-sectional area ratio of the post-pouring joint to the whole concrete deck (Γ) are selected to evaluate the influence of the age difference of the longitudinal post-pouring joint on the long-term behavior of composite beam. According to the empiric engineering practice, t_a = 180 and 360 days, and Γ = 12% and 15% were selected as typical situations for the parametric analysis. The difference of mid-span deflection, concrete stress at the top of precast slabs and steel stress at the bottom of steel girder calculated by the proposed model and traditional model, are presented in Figs. 10-12, for the case of uniform vertical load and the axial load.

As shown in Fig. 10, the difference of the deflection calculated by the two models increase rapidly under the uniform vertical load first, and then decreases gradually with time, and the difference of the deflection reaches the highest value within 180 days after the placement of concrete joint. This phenomenon can be attributed by the different shrinkage and creep performance of the precast slabs and the post-pouring joint due to the age difference. For the case of Γ = 15% and t_a = 360 days, the peak difference of deflection is 18.2%, and the difference remained above 16.3% after ten years. The difference of the deflection calculated by the two models increase with the increase of Γ and t_a. And for this case, the difference of the deflection increased about 3% for Γ increased from 12% to 15% or t_a increased from 180 to 360 days.

The phenomenon similar to Fig. 10 can be seen from

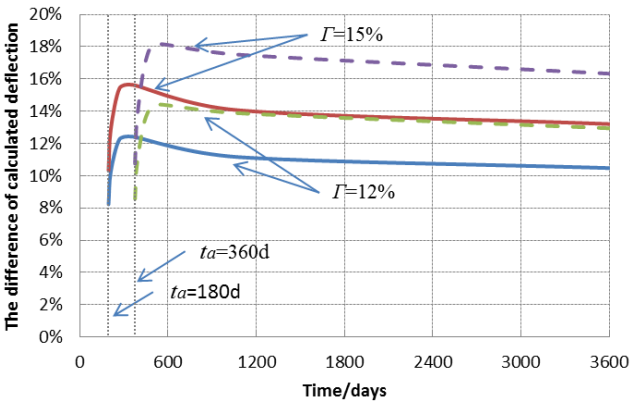

Fig. 10 The difference of the mid-span deflection calculated by the two models

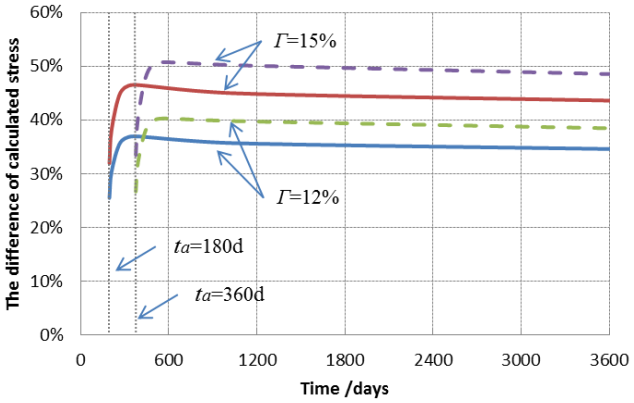

Fig. 11 The difference of the concrete stress at the top of precast slab calculated by the two models

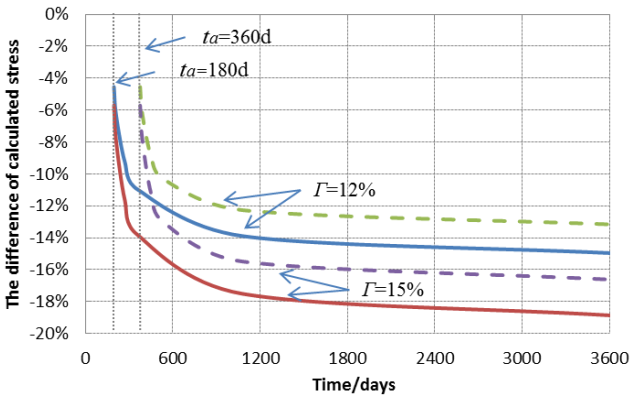

Fig. 12 The difference of the stress at the bottom of steel girder under axial load calculated by the two models

Fig. 11. It should be noted that the difference of concrete stress in the four situations by the two models reached above 35% after assembled 180 days. Especially, under the case of Γ = 15% and t_a = 360 days, the highest value of the difference of concrete stress calculated by the two models is 50.7%, and the difference remained above 48.5% after 10 years. And it indicates that the difference of the concrete stress do not decrease obviously with time after 180 days.

The influence of Γ and t_a on the difference of the concrete stress calculated by the two models is similar to those on the difference of deflection. For the case studied in the section, the difference of the concrete stress increase by about 10% for Γ increase from 12% to 15%.

It can be seen from Fig. 12 that the age difference between the precast slabs and the post-pouring joint would reduce the stress at the bottom of steel girder under axial load, which is much different from those of concrete stress and deflection. The difference of steel stress calculated by the two models increase rapidly for the assembly of precast concrete slabs, and after nearly two years increased with a gradually reduced rate. At the age of ten years, the stress of steel girder calculated by the proposed model is 13%~19% which is lower than that calculated by traditional model.

6. Conclusions

A time-dependent model of precast-assembled steel-concrete composite beam with post-pouring joint is proposed in this paper. The action of external load, steel-concrete interface slip, and the influence of shrinkage and creep of concrete deck are covered in this model. And a special attention is paid to the age difference between the precast slabs and the post-pouring joint in the proposed model. From the case study and parametric analysis presented in this paper, the following conclusions can be drawn:

- The mechanical principle of this method is clear, and this model can be used to evaluate the long-term performance of precast-assembled steel-concrete composite beams much more accurate than traditional model.
- The age effect of post-pouring joint will delay the stress attenuation trend of the concrete slab and further increased the long-term deflection. For the case of Γ = 15% and t_a = 360 days, the value for concrete stress and mid-span deflection calculated by the proposed model are 48.5% and 16.3% higher than that of the traditional model, respectively
- Tensile stress may occur in the post-pouring joint area during the construction and in-service stage. It deserves great attention from the viewpoint of life cycle design or service performance evaluation.
- The difference of concrete stress calculated by the proposed model and traditional model is sensitive to cross-sectional area ratio of the post-pouring joint to the whole concrete deck. The difference of maximum concrete stress increases by about 10% when the cross-sectional area ratio increases from 12% to 15%.

Acknowledgments

The research described in this paper was financially supported by the National Natural Science Foundation of China (No. 51378501, 51578547, 51778628).

References

Al-Deen, S., Ranzi, G. and Vrcelj, Z. (2011a), "Shrinkage effects on the flexural stiffness of composite beams with solid concrete slabs: An experimental study", *Eng. Struct.*, **33**(4), 1302-1315.

Al-Deen, S., Ranzi, G. and Vrcelj, Z. (2011b), "Full-scale long-term experiments of simply supported composite beams with solid slabs", *J. Constr. Steel Res.*, **67**(3), 308-321.

Al-Deen, S., Ranzi, G. and Uy, B. (2015), "Non-uniform shrinkage in simply-supported composite steel-concrete slabs", *Steel Compos. Struct., Int. J.*, **18**(2), 375-394.

Amadio, C. and Fragiacomo, M. (1997), "Simplified Approach to Evaluate Creep and Shrinkage Effects in Steel-Concrete Composite Beams", *J. Struct. Eng.*, **123**(9), 1153-1162.

Bazant, Z.P. (1972), "Prediction of concrete creep effects using age-adjusted effective modulus method", *ACI J.*, **69**(4), 212-217.

Deretic-Stojanovic, B. and Kostic, S.M. (2017), "A simplified matrix stiffness method for analysis of composite and prestressed beams", *Steel Compos. Struct., Int. J.*, **24**(1), 53-63.

Dezi, L., Leoni, G. and Tarantino, A.M. (1995), "Time-dependent analysis of prestressed composite beams", *J. Struct. Eng.*, **121**(4), 621-633.

Dezi, L., Gara, F. and Leoni, G. (2006), "Effective slab width in prestressed twin-girder composite decks", *J. Struct. Eng.*, **132**(9), 1358-1370.

Erkmen, R.E. and Bradford, M.A. (2011), "Time-dependent creep and shrinkage analysis of composite beams curved in-plan", *Comput. Struct.*, **89**(1), 67-77.

Fan, J.S., Nie, J.Q. and Li, Q. (2010a), "Long-Term Behavior of Composite Beams under Positive and Negative Bending (I) — Experimental Study", *J. Struct. Eng.*, **136**(7), 849-857.

Fan, J.S., Nie, J.Q. and Quan, L. (2010b), "Long-Term Behavior of Composite Beams under Positive and Negative Bending (II) — Analytical Study", *J. Struct. Eng.*, **136**(7), 858-865.

Gara, F., Ranzi, G. and Leoni, G. (2010), "Short- and long-term analytical solutions for composite beams with partial interaction and shear-lag effects", *Int. J. Steel Struct.*, **10**(4), 359-372.

Gara, F., Ranzi, G. and Leoni, G. (2011a), "Partial interaction analysis with shear-lag effects of composite bridges: A finite element implementation for design applications", *Adv. Steel Constr.*, **7**(1), 1-16.

Gara, F., Ranzi, G. and Leoni, G. (2011b), "Simplified method of analysis accounting for shear-lag effects in composite bridge decks", *J. Constr. Steel Res.*, **67**(10), 1684-1697.

Gilbert, R.I. (1989), "Time-dependent Analysis of Composite Steel-Concrete sections", *J. Struct. Eng.*, **115**(11), 2687-2705.

Gilbert, R.I. and Bradford, M.A. (1991), "Time-dependent behavior of simply-supported steel-concrete composite beams", *Magaz. Concrete Res.*, **157**(43), 265-274.

Giussani, F. and Mola, F. (2010), "Displacement Method for the Long-Term Analysis of Steel-Concrete Beams with Flexible Connection", *J. Struct. Eng.*, **136**(3), 265-274.

Jurkiewiez, B., Buzon, S. and Sieffert, J.G. (2005), "Incremental viscoelastic analysis of composite beams with partial interaction", *Comput. Struct.*, **83**(21), 1780-1791.

Nguyen, Q.H. and Hjiaj, M. (2016), "Nonlinear Time-Dependent Behavior of Composite Steel-Concrete Beams", *J. Struct. Eng.*, **142**(5), 04015175.

Nguyen, Q.H., Hjiaj, M. and Aribert, J.M.A. (2010a), "space-exact beam element for time-dependent analysis of composite members with discrete shear connection", *J. Constr. Steel Res.*, **66**(11), 1330-1338.

Nguyen, Q.H., Hjiaj, M. and Uy, B. (2010b), "Time-dependent analysis of composite beams with continuous shear connection based on a space-exact stiffness matrix", *Eng. Struct.*, **32**(9), 2902-2911.

Wu, J., Dan, M.F. and Soliman, M. (2015), "Simulating the construction process of steel-concrete composite bridges", *Steel Compos. Struct., Int. J.*, **18**(5), 1239-1258.

Xue, W.C., Ding, M., He, C. and Li, J. (2008), "Long-term behavior of prestressed composite beams at service loads for one year", *J. Struct. Eng.*, **134**(6), 930-937.

Xue, W.C., Sun, T.R. and Liu, T. (2013), "Experimental study on prestressed steel-concrete composite beams for urban light rails under sustained loads of two years", *China Civil Eng. J.*, **46**(3), 110-118. [In Chinese]

Zhu, L. and Su, R.K.L. (2017), "Analytical solutions for composite beams with slip, shear-lag and time-dependent effects", *Eng. Struct.*, **152**, 559-578.

BU